Atmos. Chem. Phys. Discuss., 13, 23781–23816, 2013
www.atmos-chem-phys-discuss.net/13/23781/2013/
doi:10.5194/acpd-13-23781-2013


Atmospheric Chemistry and Physics Discussions



# Injection heights of springtime biomass burning plumes over the Peninsular Southeast Asia and their impacts on pollutant long-range transport

**Y. Jian and T.-M. Fu**

Laboratory for Climate and Ocean-Atmosphere Studies, Department of Atmospheric and Oceanic Sciences, School of Physics, Peking University, Beijing, 100871, China

Received: 13 August 2013 – Accepted: 28 August 2013 – Published: 10 September 2013

Correspondence to: T.-M. Fu (tmfu@pku.edu.cn)

Published by Copernicus Publications on behalf of the European Geosciences Union.







## Abstract

We analyzed observations from the Multi-angle Imaging SpectroRadiometer (MISR) to determine the injection heights of biomass burning smoke plumes over the Peninsular Southeast Asia (PSEA) in spring, with the goal of evaluating the impacts on pollutant long-range transport. We retrieved the heights of twenty-two thousand MISR smoke pixels from 607 smoke plumes over the PSEA during February to April of the years 2001–2010. Forty-five percent of the analyzed smoke pixels were above the local mean boundary layer (1 km) at MISR overpass time (10:30 a.m. local time). We used the GEOS-Chem model to simulate the transport of PSEA biomass burning pollutants in March 2001. We found that the direct injection of 40 % of the PSEA biomass burning emissions had little impact on the long-range transport of CO to downwind regions, compared to a control simulation where all biomass burning emissions were released in the boundary layer. This was because CO at the surface over the PSEA was efficiently lifted into the free troposphere by deep convection associated with synoptic-scale weather systems. For pollutants with lifetimes shorter than the synoptic timescale, such as black carbon aerosol (BC), their long-range transport was much more sensitive to the initial plume injection height. The direct injection of $NO_x$ from PSEA biomass burning into the free troposphere drove increased formation and transport of PAN, which in turn led to significant increases of ozone over downwind southern China and northwestern Pacific. The Pacific subtropical high transported PSEA biomass burning pollutants to the marine boundary layer over the tropical northwestern Pacific. We compared our model results to aircraft measurements over the northwestern Pacific during the TRACE-P campaign (March 2001). The direct injection of 40 % of the PSEA biomass burning pollutants in the free troposphere in the model led to a more pronounced BC peak at 3 km over the northwestern Pacific, which was in better agreement with the aircraft observations compared to the control simulation. Our analyses highlighted the point that the injection heights of smoke plumes pose large





ACPD
13, 23781–23816, 2013



uncertainty to the interpretation of BC measurements downwind of biomass burning regions.

## 1 Introduction

Open burning of biomass emits large amounts of trace gases and aerosols into the atmosphere, affecting atmospheric chemistry and climate. Buoyed by the thermal energy of the fire and the local atmospheric instability, biomass burning smoke plumes can sometimes rise above the boundary layer and inject directly into the free troposphere, affecting the long-range transport efficiency of the emitted pollutants (e.g., Colarco et al., 2004; Fromm et al., 2005; Damoah et al., 2006). Over the Peninsular Southeast Asia (PSEA, here defined as Vietnam, Cambodia, Thailand, Laos, and Myanmar), heavy biomass burning recurs annually in spring (February to April) due to land-clearing practices before the local growing season (Fox et al., 2009). Here we analyzed space-based observations to determine the injection heights of biomass burning smoke plumes over the PSEA in spring, as well as assessed their impacts on the long-range transport of pollutants and the formation of ozone in downwind regions.

The pollutants emitted from PSEA biomass burning in spring can be transported by the prevailing westerly wind to affect the local air quality and chemistry over downwind southern China and the northwestern Pacific. Surface and ozonesonde measurements in southern China in spring showed significant enhancements in CO, black carbon aerosol (BC), $PM_{2.5}$, $PM_{10}$, and ozone when the local air was impacted by air masses back-traceable to the PSEA (Liu et al., 1999; Chan et al., 2000; Deng et al., 2008; Lin et al., 2009, 2010; Yen et al., 2012). Using a regional model, Fu et al. (2012) found that the long-range transport of PSEA biomass burning emissions during spring 2006 contributed significantly to the monthly mean surface concentrations of CO (20–50 %), ozone (10–30 %), and $PM_{2.5}$ (10–70 %) in southern China, as well as leading to 2–5 ppbv ozone enhancement in the lower troposphere over the western Pacific. Aircraft measurements along the Pacific Rim during the Transport and Chemical Evolution over





ACPD
13, 23781–23816, 2013



the Pacific (TRACE-P) campaign in spring 2001 characterized the outflow of biomass burning pollutants from the PSEA to the northwestern Pacific (Jacob et al., 2003). Over the northwestern Pacific (17°–30° N, 110°–150° E), back trajectories showed that 45 % and 60 % of the air masses sampled by TRACE-P aircrafts at 2–4 km and 4–8 km altitude, respectively, were transported from the PSEA (Kondo et al., 2004). Model simulations showed that biomass burning pollutants were lifted from the PSEA by deep convection and the warm conveyor belts ahead of cold fronts and transported to the northwestern Pacific at altitudes above 2 km (Carmichael et al., 2003; Liu et al., 2003; Miyazaki et al., 2003; Lin et al., 2009).

Model studies showed that direct injection of biomass burning pollutants into the free troposphere generally leads to enhanced long-ranged transport, due to faster transport by the stronger winds and/or prolonged lifetime of the pollutants in the free troposphere (Leung et al., 2007; Chen et al., 2009). The standard treatment in most large-scale chemical transport models has been to release biomass burning emissions in the boundary layer (e.g., Bey et al., 2001). Leung et al. (2007) and Turquety et al. (2007) simulated the transport of CO from summertime boreal forest fires. Both studies found that injecting 60 % of the biomass burning emissions directly into the free troposphere in the model improved agreement with downwind CO surface and column measurements, compared to simulations where biomass burning emissions were released only in the boundary layer. Several studies embedded high resolution models or parameterization schemes to resolve the plume-rising process in large-scale chemical transport models (Freitas et al., 2006, 2007; Rio et al., 2010). These studies also found that the injections of biomass burning emissions into the free troposphere have large impact on CO concentrations downwind (Freitas et al., 2006, 2007). Conversely, Chen et al. (2009) found that the injection heights of North American boreal fire emissions had limited impacts on CO concentrations over the downwind areas in North America. They attributed this lack of sensitivity to frequent strong convections occurring along the transport pathway, which would lift CO into the free troposphere regardless of the initial injection height. However, they showed that the long-range transport of BC was





ACPD
13, 23781–23816, 2013



much more senstive to injection height, owing to the shorter lifetime of BC compared to CO.

Space-based remote sensing, such as images from the Multi-angle Imaging SpectroRadiometer (MISR) and backscatter measurements from the Cloud-Aerosol Lidar with Orthogonal Polarization (CALIOP), can be used to determine the injection heights of biomass burning smoke plumes (e.g., Kahn et al., 2007, 2008; Labonne et al., 2007). Height-retrieval studies using MISR images showed that the injection heights of smoke plumes associated with summertime North American forest fires ranged from a few hundred meters to 5 km (Mazzoni et al., 2007; Kahn et al., 2008; Val Martin et al., 2010). Analyses of CALIOP backscattering measurements of smoke plumes from summertime European forest fires similarly found injection heights of 1.6-5.9 km (Amiridis et al., 2010). However, Labonne et al. (2007) analyzed CALIOP backscatter measurements over 8 major biomass burning regions over the world during July–August 2006. They found that the injection height for most smoke plumes were within the boundary layer, especially in the tropics. Studies indicated that the injection heights of smoke plumes are sensitive to the type of biomass burned, the thermal power of the fire, and the atmospheric stability structure at the burning site (Ferguson et al., 2003; Mims et al., 2010; Val Martin et al, 2010, 2012; Tosca et al., 2011; Zender et al., 2012).

In this study, we analyzed satellite observations over the PSEA in spring during the years 2001 to 2010 to determine the injection heights of biomass burning smoke plumes. We applied the resulting probability distribution of smoke plume injection heights to a chemical transport model to assess the impacts on the long-range transport of pollutants to downwind southern China and the northwestern Pacific. We compared model results against aircraft measurements during the TRACE-P campaign in spring 2001 to further examine the impacts on long-range transport and the interpretation of measurements.





ACPD
13, 23781–23816, 2013



## 2 Data and methodology

### 2.1 Fire observation from MISR and MODIS, and smoke plume identification using MINX

We used a two-step approach to extract MISR observations of biomass burning smoke plumes over the PSEA in spring during the years 2001 to 2010. We first used the Level 2 thermal anomalies product from the Moderate-resolution Imaging Spectroradiometer (MODIS) instrument (MOD14) (Giglio et al., 2003) to locate possible open fires over the PSEA during this period. We then extracted the MISR scenes intersecting these thermal anomalies to screen for smoke plumes.

Both MODIS and MISR are onboard the NASA Terra satellite, which overpasses the equator in the descending mode at approximately 10:30 a.m. local time. The cross-track swath width of MODIS is 2330 km, such that global coverage is achieved every one to two days. MODIS has 36 spectral channels with wavelengths between 0.4 µm and 14.2 µm. Thermal anomalies are detected at 1 km spatial resolution (nadir) using the brightness temperatures derived from the 4 µm and 11 µm channels (Giglio et al., 2003).

The MISR instrument (Diner et al., 1998) consists of nine push-broom cameras placed at viewing angles from -70.5° to 70.5° (relative to nadir) in line with the ground track. Each camera acquires data at four wavelengths: 446 nm, 558 nm, 672 nm, and 866 nm. The cross-track width of the MISR swath, common to all nine cameras, is 360 km, such that global coverage is achieved every nine days at the equator. The horizontal resolution is 275 m in the red band for all nine cameras and in all four bands for the nadir camera. The horizontal resolution for the remaining 24 bands is 1.1 km.

We manually screened for smoke plumes with the aid of the MISR INteractive eXplorer software (MINX) developed by the Jet Propulsion Laboratory (Nelson et al., 2008). MINX combines the four spectral bands to form a high-resolution true-color image for each of the nine cameras on MISR, and the resulting nine images can be animated. We used this animation, superimposed with the MODIS thermal anomalies, as





ACPD
13, 23781–23816, 2013



a visual aid to subjectively identify smoke plumes. Our criteria for identifying a biomass burning smoke plume were: (1) a plume-shaped area of high reflectivity was visible from the MINX animation; (2) that high-reflectivity area showed a shift in position relative to the surface between cameras, indicating that it was above the surface; and (3) the vertex of that high-reflectivity area was marked by one or more MODIS thermal anomalies. We manually determined the boundary and surface origin of the smoke plume, as well as the local wind direction, using the animation.

### 2.2 Smoke pixel height retrieval using MINX

We used the stereoscopic algorithm in MINX to retrieve the heights of the individual smoke pixels in the identified smoke plumes. Stereo-height retrieval is based on the shifts of pixels relative to the surface between cameras (Nelson et al., 2008). The MINX height retrieval algorithm uses data from the seven inner cameras on MISR, instead of using data from only the three center cameras as the standard MISR height retrieval algorithm does (Moroney et al., 2002). Also, MINX allows its users to specify the wind direction over the targeted area to better account for advection during the time lapses between cameras. The height of each smoke pixel was defined relative to the topography directly underneath that smoke pixel. For most smoke pixels, we used the wind-corrected stereo-height retrieved by MINX. However, the wind correction factor could not be calculated for pixels less than 226 m above the local terrain, or in scenes where the wind direction was within 15° of the instrument track. In such cases, we used the zero-wind stereo-height retrieval instead. The differences between wind-corrected stereo-height and zero-wind stereo-height, where both were retrieved, were almost always within 500 m. Only 2 % of the analyzed pixels had wind-corrected stereo-heights and zero-wind stereo-heights differing by more than 1 km. The horizontal and vertical resolutions for the pixel stereo-height retrieved by MINX were 275 m and 226 m, respectively (Nelson et al., 2008).





ACPD
13, 23781–23816, 2013



## 2.3 Land cover data

We used the MODIS Level 3 land cover product (MOD12Q1) (Friedl et al. 2010) to determine the type of land cover associated with each of the identified smoke plumes. This product was derived from a year of MODIS observations from both the Terra and Aqua platforms and contained the 17 IGBP land cover classes. The horizontal resolution of the land cover dataset was 0.5 km.

## 2.4 Model simulations

We used the GEOS-Chem global chemical transport model to simulate the transport of biomass burning pollutants from PSEA during spring 2001. GEOS-Chem (version 9.1.2; http://acmg.seas.harvard.edu/geos) was driven by the assimilated meteorological data (MERRA) from the Goddard Earth Observing System (GEOS) of the NASA Global Modeling Assimilation Office (Bey et al., 2001). The native resolution of the meteorological data was 0.67° longitude × 0.5° latitude, with 72 levels extending from the surface to 0.01 hPa. To drive our simulation, the horizontal resolution was reduced to 2.5° longitude × 2.0° latitude. Vertical levels were reduced to 47 levels, with 8 levels in the lowest 1 km and 14 levels between 1 km and 5 km. Meteorology fields were updated in the model every 3 hours (every 1 hour for surface quantities and planetary boundary layer depths, and every 6 hours for instantaneous fields). The chemistry scheme in GEOS-Chem was as described in Bey et al. (2001) and Mao et al. (2010). Vertical mixing within the boundary layer was assumed to be instantaneous (Bey et al., 2001). Convective transport was computed from the convective mass fluxes in the meteorological fields, as described by Wu et al. (2007). Dry deposition was based on Wesely (1989) as implemented by Wang et al. (1998). Wet deposition was as described by Liu et al. (2001). Freshly emitted BC was assumed to be 80 % hydrophobic and 20 % hydrophilic, with a conversion timescale from hydrophobic to hydrophilic of 1.15 days (Park et al., 2005). GEOS-Chem has been used extensively to study the long-range





ACPD
13, 23781–23816, 2013



transport of pollutants from Asia and from other parts of the world (e.g, Liu et al., 2003; Park et al., 2005; Leung et al., 2007; Turquety et al., 2007; Zhang et al., 2008).

Table 1 summarizes the emissions used in our model simulations. Biomass burning emissions from East and South Asia were taken from the inventory developed by Streets et al. (2003a), which had a native resolution of $1^\circ \times 1^\circ$ and represented average burning conditions of the mid-1990s. Annual biomass burning emissions of CO, $NO_x$, non-methane volatile organic compounds (NMVOC), and BC from PSEA were 32 Tg yr$^{-1}$, 0.33 TgN yr$^{-1}$ (as $NO_2$), 5.7 Tg yr$^{-1}$, and 0.21 TgC yr$^{-1}$, respectively. We applied monthly variations to the biomass burning emissions over East and South Asia based on the Along Track Scanning Radiometer (ATSR) satellite hot spot counts from 1996 to 2000 (Duncan et al., 2003). Over the PSEA, 82 % of the annual total biomass burning emission was emitted in spring; half of the annual emission total was emitted in March. We did not resolve daily emissions. Heald et al. (2003) showed that using monthly-resolved PSEA biomass burning emissions significantly improved the simulation of aircraft measurements downwind of the PSEA, while using daily-resolved emissions did not offer further improvement. Monthly mean biomass burning emissions for the rest of the world were taken from the Global Fire Emissions Database version 2 (GFED2) (van der Werf et al., 2006) for the year 2001. The GFED2 inventory was not used for the PSEA, because it has been shown to be significantly low-biased for this region (Fu et al., 2012).

Anthropogenic emissions for East and South Asia were taken from the inventory developed by Zhang et al. (2009), which had a native resolution of $0.5^\circ \times 0.5^\circ$ and included emissions from power generation, industry, transportation, as well as residential sources. This inventory was developed for the year 2006 but the emission totals were consistent with top-down emission estimates for CO (Heald et al., 2004) and NMVOC (Fu et al., 2007) for the year 2001. BC and $NO_x$ emission estimates were likely to be high relative to the actual emissions in the year 2001 (Zhang et al. 2009). For the PSEA, the total annual anthropogenic emissions of CO, $NO_x$, NMVOC, and BC were 20.5 Tg yr$^{-1}$, 0.59 TgN yr$^{-1}$ (as $NO_2$), 5.0 Tg yr$^{-1}$, and 0.18 TgC yr$^{-1}$, respectively. The





ACPD
13, 23781–23816, 2013



seasonal variations of emissions for the residential sector were dependent on monthly mean temperatures (Streets et al., 2003b). The monthly variations of power-generation and industrial emissions for China were based on provincial monthly activity data (Zhang et al., 2009). For the rest of the world, we used annual mean anthropogenic emissions from the EDGAR inventory for the year 2000 (Olivier and Berdowski, 2001) for CO and $NO_x$ and from the RETRO inventory for the year 2000 (Schultz et al., 2007) for NMVOCs. Biogenic VOC emissions were from the MEGAN inventory (version 2.1) (Guenther et al., 2012), with seasonal variations driven by leaf area index observations from MODIS (Myneni et al., 2002).

### 2.5 Aircraft measurements from the TRACE-P campaign

We compared our model results to aircraft measurements during the TRACE-P campaign in spring 2001 (Jacob et al., 2003). Two NASA aircrafts were deployed during the campaign: the DC-8 (12 km ceiling) and the P-3B (7-km ceiling). BC absorption was measured on both aircrafts at 565 nm using particle soot absorption photometers (Radiance Research) and corrected for scattering (Bond et al., 1999, Clark et al., 2004). We calculated BC concentrations by assuming a mass absorption efficiency of 7.5 $m^2\,g^{-1}$ (Bond et al., 2013) and converting to STP conditions. On both aircrafts, whole air samples were collected in canisters every 3–7 min during horizontal flight legs and every 1–3 min during ascents and descents. $CH_3Cl$ and $C_2Cl_4$ concentrations in these canister air samples were determined using gas chromatography (Blake et al., 2003). All measurements were merged to a time resolution of one minute.

## 3 Injection height of springtime biomass burning smoke plumes over PSEA

### 3.1 Probability distributions of smoke pixel heights

We analyzed the MODIS and MISR observations over the PSEA between February-April for the years 2001–2010 to identify the smoke plumes from biomass burning.





ACPD
13, 23781–23816, 2013



MODIS detected twenty thousand thermal anomalies in MISR footprints over the PSEA during the target time periods. Using the criteria described in Sect. 2.2, a total of 607 biomass burning smoke plumes were identified. Each identified smoke plume contained 10 to 400 smoke pixels. In all, heights were retrieved for 22 350 smoke pixels during February–April for the years 2001–2010.

Figure 1 shows the spatial distributions of the identified biomass burning smoke plumes during February-April for the years 2001 to 2010 and for the year 2001 alone. The identified smoke plumes were largely distributed over the agricultural areas near the major rivers, including the Mekong, the Chao Phraya, the Salween, and the Irrawaddy. The areas with highest densities of identified smoke plumes are northern Loas and western Myanmar. The MODIS thermal anomalies also showed a similar spatial distribution (not shown). There was no significant difference in the spatial distributions of the identified smoke plumes from year to year.

Figure 2a shows the probability distribution of the smoke pixel heights (binned into 0.5 km intervals) in spring during the years 2001 to 2010. Retrieved smoke pixel heights ranged from 0 to 6 km. 55 % of the smoke pixels were below 1 km, which was the mean local boundary layer height at Terra overpass time (10:30 a.m. local time) in the MERRA dataset. Approximately 28 % of the smoke pixels were between 1 km and 2 km, and 17 % of the smoke pixels were above 2 km. Only 1.5 % of the smoke pixels were between 4 and 5 km, and only 0.4 % of the smoke pixels were between 5 and 6 km. Overall, 45 % of the smoke pixels were above the local mean boundary layer. Figure 2a also shows the range of smoke pixel height probability for each year between 2001 and 2010. There was considerable interannual variability in the probability distribution of the smoke pixel heights. The percentage of smoke pixels above 1 km was lowest at 24 % in 2010 and highest at 58 % in 2007. The percentage of smoke pixels above 1 km was 57 % in 2001.

We found that the smoke pixel heights varied with the type of land cover burned. Figure 1 shows the land cover at the locations of each of the identified smoke plumes. Out of the 607 smoke plumes identified during 2001–2010, 64 % were over evergreen





ACPD
13, 23781–23816, 2013



and deciduous broadleaf forests, 30 % were over woody savanna, and 6 % were over cropland or cropland/natural vegetation mosaic. Figure 2b compares the probability distributions of smoke pixel heights over broadleaf forests, woody savanna, and cropland. The retrieved heights of smoke pixels over croplands were significantly lower in altitude compared to those over broadleaf forests and savanna. 76 % of the smoke pixels over croplands were below 1 km, with no pixels above 4 km. 44 % of the smoke pixels over woody savanna were above 1 km, with 1.1 % above 5 km. 47 % of the smoke pixels over broadleaf forests were above 1 km, with 0.1 % above 5 km.

### 3.2 Uncertainty analysis

The probability distributions of smoke pixel heights determined in Sect. 3.1 were susceptible to possible biases from sampling. The MISR swath is 360 km wide while the MODIS swath is 2330 km wide. As a result, 85 % of the fire pixels detected by MODIS were not within MISR footprints. In addition, fires and smoke plumes obscured by clouds were not detected by either MODIS or MISR. We assumed that the smoke plumes outside of MISR footprints or obscured by clouds had the same smoke pixel height distribution as the ones analyzed in Sect. 3.1.

Additional uncertainty in the smoke pixel height probability distribution may come from the under-identification of small/low plumes. In our analysis, only half of the MODIS thermal anomalies within MISR footprints were associated with a visible smoke plume. Some of the thermal anomalies without visible smoke plumes may be false detection due to sun glint, hot desert surface, coasts, or clouds (Giglio et al. 2003). However, it was also possible that smoke plumes that were small or close to the surface were not visible to our eyes in the MISR imageries due to their low reflectivity contrast. To assess this bias, we analyzed the number of thermal anomalies associated with each of the identified smoke plumes in spring 2010. We found that each of the identified smoke plumes was associated with a range of 1 to 12 MODIS thermal anomalies at the vertex of the plume. The thermal anomalies not associated with visible smoke plumes were in most cases stand-alone. We assumed that these stand-alone thermal





ACPD
13, 23781–23816, 2013



anomalies were detected falsely or associated with very small fires with little emission. To each cluster of more than two MODIS thermal anomalies but without a visible smoke plume, we assigned 5 smoke pixels (half the smallest number of smoke pixels in identified plumes), each with a height < 500 m (the lowest altitude bin in Fig. 2). A total of 105 smoke pixels were thus assigned. The resulting difference in the overall probability of smoke pixel height below 1 km was less than 3 %, and we ignored this source of error henceforth.

## 4 Impacts of smoke injection height on pollutant long-range transport and ozone formation

### 4.1 Long-range transport of CO

We used the GEOS-Chem model to simulate the outflow of PSEA biomass burning pollutants in spring 2001 and assessed the impacts of smoke plume injection heights on the long-range transport of pollutants. Two simulations were conducted. In the control simulation, all biomass burning emissions were released evenly within the boundary layer following the standard practice in GEOS-Chem. In the sensitivity simulation, the biomass burning emissions over the PSEA were released according to the probability distribution of smoke pixel heights observed by MISR for the year 2001. That is, 40 % of the PSEA biomass burning emission was released in the model evenly between the top of the local boundary layer and 5 km altitude, while the remaining 60 % was released in the boundary layer. Both simulations were conducted from July 2000 to April 2001. The first eight months spun up the model. Below we focused on March 2001, when the biomass burning emission from the PSEA was at its peak. Figure 3 shows the biomass burning emission of CO for March 2001. Emissions were high over the entire PSEA with largest fluxes exceeding $5 \times 10^{12}$ molecules $cm^{-2}$ $s^{-1}$ over northern Laos and western Myanmar, consistent with the locations of smoke plumes observed by MISR (Fig. 1).





ACPD
13, 23781–23816, 2013



Figure 4a and b show the monthly mean CO concentrations in March 2001 in the control simulation, as well as the fraction contributed by PSEA biomass burning and the monthly mean wind fields, at five different altitudes. At the surface, highest CO concentrations exceeding 500 ppb were found over the PSEA, where the local biomass burning emissions contributed 40–70 % of the surface CO. PSEA biomass burning emissions also contributed 5–20 % of surface CO over southwestern China, but otherwise had little impact on the surface CO concentrations over the rest of East Asia. At 850 hPa, the area most affected by PSEA biomass burning emissions remained over the PSEA, indicating that the emitted pollutants were largely transported vertically between the surface and 850 hPa over the PSEA in the control simulation. At 700 hPa and above, however, the area most affected by PSEA biomass burning emissions shifted northwestward to southern China and extended to the northwestern Pacific, reflecting the transport by the southwesterly to westerly wind at this altitude. Over southern China and the northwestern Pacific, PSEA biomass burning contribution was most prominent at 700 hPa, consistent with previous ozonesonde and aircraft observations of the PSEA outflows (Liu et al., 1999; Chan et al., 2000; Carmichael et al., 2003).

Figure 4c shows the percent changes of the monthly mean CO concentrations in the MISR-constrained simulation relative to the control simulation. We found that directly injecting PSEA biomass burning pollutants into the free troposphere had only a small impact on the long-range transport of CO. Over the PSEA source region, CO concentrations decreased by 10–15 % at the surface and increased by 5–15 % at 700 hPa, reflecting the direct injection of CO into the free troposphere in the MISR-constrained simulation. However, downwind, CO concentrations increased by less than 10 % over southern China at 700 hPa and less than 5 % over the northwestern Pacific at 700 hPa, with no significant changes elsewhere. Figure 5a shows the percent differences of tropospheric column CO burden in the MISR-constrained simulation relative to the control simulation. The direct injection of PSEA smoke plumes into the free troposphere led to less than 5 % decrease in the CO burden over the source region and less than 5 % increase in the CO burden over southern China.





ACPD
13, 23781–23816, 2013



Why was the long-range transport of biomass burning CO from the PSEA insensitive to the smoke plume injection height? We found that the surface circulation over the PSEA in March was dominated by a persisting low-pressure system (Fig. 4b), which converged surface air and induced deep convection over the region. That deep convection was enhanced by the passage of cold fronts associated with midlatitude cyclones every 2–7 days (Liu et al., 2003). Therefore, CO, which has a mean lifetime of two months, was efficiently lifted by these synoptic-scale processes from the surface to 2–3 km, where it was subsequently transported downwind by the persistent westerly. We concluded that for PSEA biomass burning pollutants with lifetime significantly longer than 7 days (the synoptic timescale), their long-range transport were relatively insensitive to the plume injection heights. This finding was similar to that of Chen et al. (2009) for North American boreal fire emissions.

### 4.2 Impacts on the long-range transport of BC, $NO_x$, and PAN, and the formation of ozone

Figure 6a shows the percent changes of BC concentrations in the MISR-constrained simulation relative to the control simulation during March 2001. We found that the long-range transport of BC was more sensitive to the smoke plume injection height than that of CO. Over the PSEA, surface BC concentrations decreased by 20–40 %, reflecting the smaller amount of biomass burning released at the surface in the MISR-constrained simulation. At 700 hPa, the increases in BC concentrations as a result of the direct injection of BC pollutants into the free troposphere were 50–100 %, much larger than those for CO. BC over the PSEA was removed by wet scavenging at a timescale of 4 days. As a result, surface BC was not as efficiently transported to the free troposphere by deep convection, such that the impact of direct injection into the free troposphere was more pronounced. Subsequent eastward transport of BC to southern China and the northwestern Pacific between 15° N–25° N increased by as much as 70 % at 700 hPa and by 20–40 % at 500 hPa. Interestingly, BC concentrations also increased significantly by 10–40 % at low altitudes (surface to 850 hPa) over the tropical





ACPD
13, 23781–23816, 2013



northwestern Pacific (5° N–15° N, 130° E–160° E), where the prevailing wind was easterly. We found that this was due to the increased transport of BC to the northwestern Pacific (15° N–25° N) between 700 hPa and 500 hPa. Part of those BC were then transported clockwise by the Pacific subtropical high pressure system and carried to lower altitude by the subsiding northeasterly flow between 5° N–15° N (Fig. 6a).

Figure 6 also shows the percent changes of $NO_x$, PAN, and ozone concentrations in the MISR-constrained simulation relative to the control simulation. The photochemical lifetime of $NO_x$ in the lower troposphere is several hours, much shorter than the timescale of deep convection. Therefore, the vertical profile of $NO_x$ over the source region was also sensitive to the injection height of smoke plume. As seen in Fig. 6b, $NO_x$ concentrations over the PSEA decreased by 20–30 % at the surface and increased by 100–200 % at 700 hPa. This change in $NO_x$ then drove changes in the formation of PAN (Fig. 6c), such that PAN concentrations over the PSEA decreased by 10–20 % at the surface and increased by 40–70 % at 700 hPa. The lifetime of PAN against thermal decomposition at 700 hPa is several months, much longer than its lifetime at the surface (approximately one hour). Therefore, at 700 hPa PAN can be efficiently transported over large distances. Figure 6c shows that the eastward transport of PAN between 15° N–25° N at 700 hPa increased by 10–30 %, reaching as far east as 180° E. Similar to the case of BC, at around 180° E at 700 hPa the wind direction changed to northeasterly and then easterly as part of the clockwise flow of the Pacific subtropical high. The transported PAN thermally decomposed to $NO_x$ in the subsiding northeasterly flow below 15° N to produce $NO_x$ over the tropical northwestern Pacific below 850 hPa. Due to the increase of $NO_x$ and PAN, ozone increased by 5–20 % at 700 hPa over the PSEA and the downwind southern China and northwestern Pacific (Fig. 6d). There was also a small ozone enhancement of approximately 5 % over the tropical northwestern Pacific below 850 hPa produced from $NO_x$ from the thermally-decomposed PAN.

Figure 5 shows the percent changes of the column burden of BC, $NO_x$, PAN, and ozone in the MISR-constrained simulation relative to the control simulation. The tropospheric BC burden was most sensitive to the smoke plume injection height. How-





ACPD
13, 23781–23816, 2013



ever, the area of largest BC percent enhancement was not over southern China or the northwestern Pacific immediately downwind from the PSEA, but over the tropical northwestern Pacific (5° N–15° N). As discussed above, the direct injection of BC into the free troposphere resulted in an increased BC outflow between 15° N-25° N at 700 hPa, which was then transported clockwise by the Pacific subtropical high. Convection was suppressed in the subsiding northeasterly between 5° N–15° N, such that BC lifetime was lengthened. As a result, BC burden increased by 15–20 % (from 21 $\mu g\,m^{-2}$ to 49 $\mu g\,m^{-2}$) in the remote atmosphere over the tropical northwestern Pacific. To the best of our knowledge, this transport pathway of PSEA pollutants to the tropical northwestern Pacific in spring has not been reported previously. The BC thus transported can possibly impact the marine boundary layer dynamics through its semi-direct radiative effect (Koch and Del Genio, 2010) and warrants further investigation. The clockwise flow of the Pacific subtropical high also drove the long-range transport of PAN. The column burden of PAN increased by up to 10 % between 10° N–20° N in the northwestern Pacific, leading to the increases of $NO_x$ and ozone burdens by a few percent each.

## 5 Comparison with TRACE-P aircraft measurements

Our model simulations in Sect. 4 showed that the long-range transport of PSEA biomass burning BC to the northwestern Pacific was highly sensitive to the smoke plume injection height. Here we compared model results against TRACE-P aircraft measurements over the northwestern Pacific (south of 25° N). Figure 3 shows the location of aircraft measurements used in our analysis. We sampled the model along the flight tracks at 1 min intervals. Measurements and model results were both averaged to the temporal (15 min) and spatial resolution of the model for comparison. Intercomparison flights during TRACE-P showed that the aerosol absorption measurements on the DC-8 were systematically higher than that on the P-3B (Moore et al., 2004). We examined the data from the two aircrafts separately.





ACPD
13, 23781–23816, 2013



Figure 7a, b compare the observed and simulated vertical profiles of BC concentrations in all air masses sampled by the aircrafts. On both aircrafts, measured BC concentrations were less than 1.1 $\mu g\,m^{-3}$ below 2 km, increased sharply to > 1.4 $\mu g\,m^{-3}$ around 3 km, and decreased to < 0.3 $\mu g\,m^{-3}$ above 4 km. The local maximum of BC concentrations at 2–3 km (1.4 $\mu g\,m^{-3}$ on the DC-8 and 1.7 $\mu g\,m^{-3}$ on the P-3B) reflected the altitude of the outflow from the PSEA, as shown previously in the back trajectory analysis by Kondo et al. (2004). Both the control simulation and the MISR-constrained simulation reproduced the general features of the observed vertical profiles. The BC concentrations below 2 km and above 4 km in the two simulations were almost identical. However, by directly injecting 40 % of the PSEA biomass burning BC into the free troposphere, the simulated BC concentrations increased by 15 % and 17 % at 2–3 km respectively and were closer to the aircraft measurements.

We further compared model results against the measured BC concentrations only in air masses significantly impacted by biomass burning emissions (Fig. 7c, d), determined based on the criteria that measured $CH_3Cl$ >550 ppt and $C_2Cl_4$ < 3 ppt following Kondo et al. (2004). There was no measurement below 2 km on both aircrafts. Measured BC concentrations on both aircrafts were highest at approximately 3 km (5 $\mu g\,m^{-3}$ on the DC-8 and 1.2 $\mu g\,m^{-3}$ on the P-3B) then decreased to < 0.2 $\mu g\,m^{-3}$ above 4 km. Both the control simulation and the MISR-constrained simulation reproduced the shape of the observed BC vertical profiles. Both simulations underestimated the observed high concentrations at 2–4 km. However, the MISR-constrained simulation was 57 % and 110 % higher than the control simulation and closer to the observations at 2–4 km on the DC-8 and on the P-3B.

Our analyses above showed that directly injecting 40 % of the PSEA biomass burning pollutants in the free troposphere in the model led to a more pronounced BC peak at 3 km over the northwestern Pacific, which was in better agreement with the aircraft observations compared to the control simulation. Other factors may contribute to the improved performance when using the MISR-constrained injection height, such as an underestimation of the PSEA biomass burning emissions, or an overestimation of





ACPD
13, 23781–23816, 2013



the BC wet scavenging rate in the model. Nevertheless, our analysis showed that the injection heights derived in this study based on MISR observations were consistent with available aircraft observations. More importantly, it highlighted the point that the injection heights of smoke plumes pose large uncertainty to the interpretation of BC measurements downwind of biomass burning regions. In particular, discrepancies between model and measurements cannot be attributed solely to errors in the biomass burning emission inventory, unless the impacts of plume injection heights have been addressed.

## 6 Conclusion

We analyzed satellite observations to determine the injection heights of biomass burning smoke plumes over the PSEA in spring, with the goal of assessing the impacts of smoke injection heights on pollutant long-range transport. We retrieved the heights of 22 350 smoke pixels during February to April of the years 2001 to 2010. On average, 45 % of the smoke pixels were above the mean local boundary layer top (1 km) at satellite overpass time.

We simulated the long-range transport of biomass burning pollutants from the PSEA using the GEOS-Chem model. We conducted a control simulation where all PSEA biomass burning emissions were released in the boundary layer, as well as a sensitivity simulation where 40 % of the PSEA biomass burning emissions were injected into the free troposphere. We found that the surface air over the PSEA in March was well ventilated by deep convections triggered by synoptic-scale weather systems, such that the long-range transport of pollutants with lifetime significantly longer than 7 days (e.g., CO) was relatively insensitive to the smoke plume injection heights.

The long-range transport of shorter-lived pollutants was much more sensitive to the smoke plume injection height. The eastward transport of BC to southern China and the northwestern Pacific increased by 20–70 % at 700 hPa. BC concentrations also increased significantly at low altitudes over the tropical northwestern Pacific, due to





ACPD
13, 23781–23816, 2013



transport by the Pacific subtropical high pressure system. The direct injection of PSEA biomass burning $NO_x$ into the free troposphere drove increased formation and transport of PAN, which in turn led to 5–20 % increase of ozone over downwind southern China and northwestern Pacific at 700 hPa.

We compared our model results to aircraft measurements over the northwestern Pacific during the TRACE-P campaign (March 2001). The direct injection of 40 % of the PSEA biomass burning pollutants in the free troposphere in the model led to a more pronounced BC peak at 3 km over the tropical northwestern Pacific, which was in better agreement with the aircraft observations compare to the control simulation.

Our results showed that the smoke plume injection heights pose large uncertainty to the interpretation of short-lived species measurements downwind of biomass burning regions. Discrepancies between model and measurements cannot be attributed solely to errors in the biomass burning emission estimates, unless the impacts of plume injection heights have been addressed.

*Acknowledgements.* This work was funded by the National Natural Science Foundation of China (41222035, 41175101).

## References

Amiridis, V., Giannakaki, E., Balis, D. S., Gerasopoulos, E., Pytharoulis, I., Zanis, P., Kazadzis, S., Melas, D., and Zerefos, C.: Smoke injection heights from agricultural burning in Eastern Europe as seen by CALIPSO, Atmos. Chem. Phys., 10, 11567–11576, doi:10.5194/acp-10-11567-2010, 2010.

Bey, I., Jacob, D. J., Yantosca, R. M., Logan, J. A., Field, B. D., Fiore, A. M., Li, Q. B., Liu, H. G. Y., Mickley, L. J., and Schultz, M. G.: Global modeling of tropospheric chemistry with assimilated meteorology: Model description and evaluation, J. Geophys. Res., 106, 23073–23095, doi:10.1029/2001JD000807, 2001.

Blake, N. J., Blake, D. R., Simpson, I. J., Meinardi, S., Swanson, A. L., Lopez, J. P., Katzenstein, A. S., Barletta, B., Shirai, T., Atlas, E., Sachse, G., Avery, M., Vay, S., Fuelberg, H. E., Kiley, C. M., Kita, K., and Rowland, F. S.: NMHCs and halocarbons in Asian continental outflow





ACPD
13, 23781–23816, 2013



during the Transport and Chemical Evolution over the Pacific (TRACE-P) Field Campaign: Comparison With PEM-West B, J. Geophys. Res., 108, 8806, doi:10.1029/2002JD003367, 2003.

Bond, T. C., Anderson, T. L., and Campbell, D.: Calibration and intercomparison of filter-based measurements of visible light absorption by aerosols, Aerosol Sci. Technol., 30, 582–600, doi:10.1080/027868299304435, 1999.

Bond, T. C., Doherty, S. J., Fahey, D. W., Forster, P. M., Berntsen, T., DeAngelo, B. J., Flanner, M. G., Ghan, S., Kärcher, B., Koch, D., Kinne, S., Kondo, Y., Quinn, P. K., Sarofim, M. C., Schultz, M. G., Venkataraman, C., Zhang, H., Zhang, S., Bellouin, N., Guttikunda, S. K., Hopke, P. K., Jacobson, M. Z., Kaiser, J.W., Klimont, Z., Lohmann, U., Schwarz, J. P., Shindell, D., Storelvmo, T., Warren, S. G., and Zender, C. S.: Bounding the role of black carbon in the climate system: a scientific assessment, J. Geophys. Res., 118, 5380–5552, doi:10.1002/jgrd.50171, 2013.

Carmichael, G. R., Tang, Y., Kurata, G., Uno, I., Streets, D., Woo, J. H., Huang, H., Yienger, J., Lefer, B., Shetter, R., Blake, D., Atlas, E., Fried, A., Apel, E., Eisele, F., Cantrell, C., Avery, M., Barrick, J., Sachse, G., Brune, W., Sandholm, S., Kondo, Y., Singh, H., Talbot, R., Bandy, A., Thorton, D., Clarke, A., and Heikes, B.: Regional-scale chemical transport modeling in support of the analysis of observations obtained during the TRACE-P experiment, J. Geophys. Res., 108, 8823, doi:10.1029/2002JD003117, 2003.

Chan, L. Y., Chan, C. Y., Liu, H. Y., Christopher, S., Oltmans, S. J., and Harris, J. M.: A case study on the biomass burning in southeast Asia and enhancement of tropospheric ozone over Hong Kong, Geophys. Res. Lett., 27, 1479–1482, doi:10.1029/1999GL010855, 2000.

Chen, Y., Li, Q., Randerson, J. T., Lyons, E. A., Kahn, R. A., Nelson, D. L., and Diner, D. J.: The sensitivity of CO and aerosol transport to the temporal and vertical distribution of North American boreal fire emissions, Atmos. Chem. Phys., 9, 6559–6580, doi:10.5194/acp-9-6559-2009, 2009.

Clarke, A. D., Shinozuka, Y., Kapustin, V. N., Howell, S., Huebert, B., Doherty, S., Anderson, T., Covert, D., Anderson, J., Hua, X., Moore, K. G., McNaughton, C., Carmichael, G., and Weber, R.: Size distributions and mixtures of dust and black carbon aerosol in Asian outflow: physiochemistry and optical properties, J. Geophys. Res., 119, D15S09, doi:10.1029/2003JD004378, 2004.

Colarco, P., Schoeberl, M., Doddridge, B., Marufu, L., Torres, O., and Welton, E.: Transport of smoke from Canadian forest fires to the surface near Washington, D.C.: In-





ACPD
13, 23781–23816, 2013



jection height, entrainment, and optical properties, J. Geophys. Res., 109, D06203, doi:10.1029/2003JD004248, 2004.
Damoah, R., Spichtinger, N., Servranckx, R., Fromm, M., Eloranta, E. W., Razenkov, I. A., James, P., Shulski, M., Forster, C., and Stohl, A.: A case study of pyro-convection using transport model and remote sensing data, Atmos. Chem. Phys., 6, 173–185, doi:10.5194/acp-6-173-2006, 2006.
Deng, X., Tie, X., Zhou, X., Wo, D., Zhong, L., Tan, H., Li, F., Huang, X., Bi, X., and Deng, T.: Effects of Southeast Asia biomass burning on aerosols and ozone concentrations over the Pearl River Delta (PRD) region, Atmos. Environ., 42, 8493–8501, doi:10.1016/j.atmosenv.2008.08.013, 2008.
Diner, D. J., Beckert, J. C., Reilly, T. H., Bruegge, C. J., Conel, J. E., Kahn, R. A., Martonchik, J. V., Ackerman, T. P., Davies, R., Gerstl, S. A. W., Gordon, H. R., Muller, J. P., Myneni, R. B., Sellers, P. J., Pinty, B., and Verstraete, M. M.: Multi-angle Imaging SpectroRadiometer (MISR) instrument description and experiment overview, IEEE Trans. Geosci. Remote Sens., 36, 1072–1087, doi:10.1109/36.700992, 1998.
Duncan, B. N., Martin, R. V., Staudt, A. C, Yevich, R., and Logan, J. A.: Interannual and seasonal variability of biomass burning emissions constrained by satellite observations, J. Geophys. Res., 108, 4100, doi:1029/2002JD002378.
Ferguson, S. A., Collins, R. L., Ruthford, J., and Fukuda, M.: Vertical distribution of nighttime smoke following a wildland biomass fire in boreal Alaska, J. Geophys. Res., 108, 4743, doi:10.1029/2002JD003324, 2003.
Fox, J., Fujita, Y., Ngidang, D., Peluso, N., Potter, L., Sakuntaladewi, N., Sturgeon, J., and Thomas, D.: Policies, Political-Economy, and Swidden in Southeast Asia, Human Ecology, 37, 305-322, doi:10.1007/s10745-009-9240-7, 2009.
Freitas, S. R., Longo, K. M., and Andreae, M. O.: Impact of including the plume rise of vegetation fires in numerical simulations of associated atmospheric pollutants, Geophys. Res. Lett., 33, L17808, doi:10.1029/2006GL026608, 2006.
Freitas, S. R., Longo, K. M., Chatfield, R., Latham, D., Silva Dias, M. A. F., Andreae, M. O., Prins, E., Santos, J. C., Gielow, R., and Carvalho Jr., J. A.: Including the sub-grid scale plume rise of vegetation fires in low resolution atmospheric transport models, Atmos. Chem. Phys., 7, 3385–3398, doi:10.5194/acp-7-3385-2007, 2007.





ACPD
13, 23781–23816, 2013



Friedl, M. A., Sulla-Menashe, D., Tan, B., Schneider, A., Ramankutty, N., Sibley, A., and Huang, X.: MODIS Collection 5 global land cover: Algorithm refinements and characterization of new datasets, Remote Sens. Environ., 114, 168–182, doi:10.1016/j.rse.2009.08.016, 2010.

Fromm, M., Bevilacqua, R., Servranckx, R., Rosen, J., Thayer, J. P., Herman, J., and Larko, D.: Pyro-cumulonimbus injection of smoke to the stratosphere: Observations and impact of a super blowup in northwestern Canada on 3–4 August 1998, J. Geophys. Res., 110, D08205, doi:10.1029/2004JD005350, 2005.

Fu, T.-M., Jacob, D. J., Palmer, P. I., Chance, K., Wang, Y. X., Barletta, B., Blake, D. R., Stanton, J. C., and Pilling, M. J.: Space-based formaldehyde measurements as constraints on volatile organic compound emissions in east and south Asia and implications for ozone, J. Geophys. Res., 112, D06312, doi:10.1029/2006JD007853, 2007.

Fu, J. S., Hsu, N. C., Gao, Y., Huang, K., Li, C., Lin, N.-H., and Tsay, S.-C.: Evaluating the influences of biomass burning during 2006 BASE-ASIA: a regional chemical transport modeling, Atmos. Chem. Phys., 12, 3837–3855, doi:10.5194/acp-12-3837-2012, 2012.

Giglio, L., Descloitres, J., Justice, C. O., and Kaufman, Y. J.: An enhanced contextual fire detection algorithm for MODIS, Remote Sens. Environ., 87, 273–282, doi:10.1016/S0034-4257(03)00184-6, 2003.

Guenther, A. B., Jiang, X., Heald, C. L., Sakulyanontvittaya, T., Duhl, T., Emmons, L. K., and Wang, X.: The Model of Emissions of Gases and Aerosols from Nature version 2.1 (MEGAN2.1): an extended and updated framework for modeling biogenic emissions, Geosci. Model Dev., 5, 1471–1492, doi:10.5194/gmd-5-1471-2012, 2012.

Heald, C. L., Jacob, D. J., Palmer, P. I., Evans, M. J., Sachse, G. W., Singh, H. B., and Blake, D. R.: Biomass burning emission inventory with daily resolution: application to aircraft observations of Asian outflow, J. Geophys. Res.-Atmos., 108, 8811, doi:10.1029/2002JD003082, 2003.

Heald, C. L., Jacob, D. J., Jones, D. B., Palmer, P. I., Logan, J. A., Streets, D., Sachse, G. W., Gille, J. C., Hoffman, R. N., and Nehrkorn, T.: Comparative inverse analysis of satellite (MOPITT) and aircraft (TRACE-P) observations to estimate Asian sources of carbon monoxide, J. Geophys. Res., 109, D23306, doi:10.1029/2004JD005185, 2004.

Jacob, D. J., Crawford, J. H., Kleb, M. M., Connors, V. S., Bendura, R. J., Raper, J. L., Sachse, G. W., Gille, J. C., Emmons, L., and Heald, C. L.: Transport and Chemical Evolution over the Pacific (TRACE-P) aircraft mission: Design, execution, and first results, J. Geophys. Res., 108, 9000, doi:10.1029/2002JD003276, 2003.





ACPD
13, 23781–23816, 2013



Kahn, R. A., Li, W.-H., Moroney, C., Diner, D. J., Martonchik, J. V., and Fishbein, E.: Aerosol source plume physical characteristics from space-based multiangle imaging, J. Geophys. Res., 112, D11205, doi:10.1029/2006JD007647, 2007.

Kahn, R. A., Chen, Y., Nelson, D. L., Leung, F. Y., Li, Q. B., Diner, D. J., and Logan, J. A.: Wildfire smoke injection heights: two perspectives from space, Geophys. Res. Lett., 35, L04809, doi:10.1029/2007GL032165, 2008.

Koch, D., and Del Genio, A. D.: Black carbon semi-direct effects on cloud cover: review and synthesis, Atmos. Phys. Chem., 10, 7685–7696, doi:10.5194/acp-10-7685-2010, 2010.

Kondo, Y., Morino, Y., Takegawa, N., Koike, M., Kita, K., Miyazaki, Y., Sachse, G. W., Vay, S. A., Avery, M. A., Flocke, F., Weinheimer, A. J., Eisele, F. L., Zondlo, M. A., Weber, R. J., Singh, H. B., Chen, G., Crawford, J., Blake, D. R., Fuelberg, H. E., Clarke, A. D., Talbot, R. W., Sandholm, S. T., Browell, E. V., Streets, D. G., and Liley, B.: Impacts of biomass burning in Southeast Asia on ozone and reactive nitrogen over the western Pacific in spring, J. Geophys. Res., 109, D15S12, doi:10.1029/2003JD004203, 2004.

Labonne, M., Breon, F. M., and Chevallier, F.: Injection height of biomass burning aerosols as seen from a spaceborne lidar, Geophys. Res. Lett., 34, L11806, doi:10.1029/2007GL029311, 2007.

Leung, F.-Y. T., Logan, J. A., Park, R., Hyer, E., Kasischke, E., Streets, D., and Yurganov, L.: Impacts of enhanced biomass burning in the boreal forests in 1998 on tropospheric chemistry and the sensitivity of model results to the injection height of emissions, J. Geophys. Res., 112, D10313, doi:10.1029/2006JD008132, 2007.

Lin, C.-Y., Chang, C.-C., Chan, C. Y., Kuo, C. H., Chen, W.-C., Chu, D. A., and Liu, S. C.: Characteristics of springtime profiles and sources of ozone in the low troposphere over northern Taiwan, Atmos. Environ., 44, 182–193, doi:10.1016/j.atmosenv.2009.10.020, 2010.

Lin, C.-Y., Hsu, H., Lee, Y. H., Kuo, C. H., Sheng, Y.-F., and Chu, D. A.: A new transport mechanism of biomass burning from Indochina as identified by modeling studies, Atmos. Chem. Phys., 9, 7901–7911, doi:10.5194/acp-9-7901-2009, 2009.

Liu, H., Chang, W. L., Oltmans, S. J., Chan, L. Y., and Harris, J. M.: On springtime high ozone events in the lower troposphere from Southeast Asian biomass burning, Atmos. Environ., 33, 2403-2410, doi:10.1016/S1352-2310(98)00357-4, 1999.

Liu, H. Y., Jacob, D. J., Bey, I., and Yantosca, R. M.: Constraints from Pb-210 and Be-7 on wet deposition and transport in a global three-dimensional chemical tracer model driven by assimilated meteorological fields, J. Geophys. Res., 106, 12109–12128, 2001.





ACPD
13, 23781–23816, 2013



Liu, H. Y., Jacob, D. J., Bey, I., Yantosca, R. M., Duncan, B. N., and Sachse, G. W.: Transport pathways for Asian pollution outflow over the Pacific: Interannual and seasonal variations, J. Geophys. Res., 108, 8786, doi:10.1029/2002JD003102, 2003.

Mao, J., Jacob, D. J., Evans, M. J., Olson, J. R., Ren, X., Brune, W. H., St Clair, J. M., Crounse, J. D., Spencer, K. M., Beaver, M. R., Wennberg, P. O., Cubison, M. J., Jimenez, J. L., Fried, A., Weibring, P., Walega, J. G., Hall, S. R., Weinheimer, A. J., Cohen, R. C., Chen, G., Crawford, J. H., McNaughton, C., Clarke, A. D., Jaegle, L., Fisher, J. A., Yantosca, R. M., Le Sager, P., and Carouge, C.: Chemistry of hydrogen oxide radicals (HOx) in the Arctic troposphere in spring, Atmos. Chem. Phys., 10, 5823–5838, doi:10.5194/acp-10-5823-2010, 2010.

Mazzoni, D., Logan, J. A., Diner, D., Kahn, R., Tong, L. L., and Li, Q. B.: A data-mining approach to associating MISR smoke plume heights with MODIS fire measurements, Remote Sens. Environ., 107, 138–148, doi:10.1016/j.rse.2006.08.014, 2007.

Mims, S. R., Kahn, R. A., Moroney, C. M., Gaitley, B. J., Nelson, D. L., and Garay, M. J.: MISR Stereo heights of grassland fire smoke plumes in Australia, IEEE Trans. Geosci. Remote Sens., 48, 25–35, doi:10.1109/TGRS.2009.2027114, 2010.

Miyazaki, Y., Kondo, Y., Koike, M., Fuelberg, H. E., Kiley, C. M., Kita, K., Takegawa, N., Sachse, G. W., Flocke, F., Weinheimer, A. J., Singh, H. B., Eisele, F. L., Zondlo, M., Talbot, R. W., Sandholm, S. T., Avery, M. A., and Blake, D. R.: Synoptic-scale transport of reactive nitrogen over the western Pacific in spring, J. Geophys. Res., 108, 8788, doi:10.1029/2002JD003248, 2003.

Moore, K. G., Clarke, A. D., Kapustin, V. N., McNaughton, C., Anderson, B. E., Winstead, E. L., Weber, R., Ma, Y., Lee, Y. N., Talbot, R., Dibb, J., Anderson, T., Doherty, S., Covert, D., and Rogers, D.: A comparison of similar aerosol measurements made on the NASA P3-B, DC-8, and NSFC-130 aircraft during TRACE-P and ACE-Asia, J. Geophys. Res., 109, D15S15, doi:10.1029/2003jd003543, 2004.

Moroney, C., Davies, R., and Muller, J. P.: Operational retrieval of cloud-top heights using MISR data, Ieee T Geosci Remote, 40, 1532–1540, doi:10.1109/TGRS.2002.801150, 2002.

Myneni, R. B., Hoffman, S., Knyazikhin, Y., Privette, J. L., Glassy, J., Tian, Y., Wang, Y., Song, X., Zhang, Y., Smith, G. R., Lotsch, A., Friedl, M., Morisette, J. T., Votava, P., Nemani, R. R., and Running, S. W.: Global products of vegetation leaf area and fraction absorbed PAR from year one of MODIS data, Remote Sens Environ, 83, 214–231, doi:10.1016/s0034-4257(02)00074-3, 2002.





ACPD
13, 23781–23816, 2013



Nelson, D. L., Chen, Y., Kahn, R. A., Diner, D. J. and Mazzoni, D.: Example applications of the MISR INteractive eXplorer (MINX) software tool to wild?re smoke plume analyses, in: SPIE 7089 Remote Sensing of Fire: Science and Application, San Diego, USA, 27 August 2008, 708–909, 2008.

Olivier, J. G. J., and Berdowski, J. J. M.: Global emissions sources and sinks, in: The Climate System, edited by: Berdowski, J., Guicherit, R., and Heij, B. J., A. A. Balkema Publishers/Swets & Zeitlinger Publishers, Lisse, The Netherlands, 33–78, 2001.

Park, R. J., Jacob, D. J., Palmer, P. I., Clarke, A. D., Weber, R. J., Zondlo, M. A., Eisele, F. L., Bandy, A. R., Thornton, D. C., Sachse, G. W., and Bond, T. C.: Export efficiency of black carbon aerosol in continental outflow: Global implications, J Geophys Res, 110, D11205, doi:10.1029/2004JD005432, 2005.

Rio, C., Hourdin, F., and Chédin, A.: Numerical simulation of tropospheric injection of biomass burning products by pyro-thermal plumes, Atmos. Chem. Phys., 10, 3463–3478, doi:10.5194/acp-10-3463-2010, 2010.

Schultz, M., Backman, L., Balkanski, Y., Bjoerndalsaeter, S., Brand, R., Burrows, J., Dalsoeren, S., de Vasconcelos, M., Grodtmann, B., Hauglustaine, D., Heil, A., Hoelzemann, J., Isaksen, I., Kaurola, J., Knorr, W., Ladstaetter-Weienmayer, A., Mota, B., Oom, D., Pacyna, J., Panasiuk, D., Pereira, J., Pulles, T., Pyle, J., Rast, S., Richter, A., Savage, N., Schnadt, C., Schulz, M., Spessa, A., Staehelin, J., Sundet, J., Szopa, S., Thonicke, K., van het Bolscher, M., van Noije, T., van Velthoven, P., Vik, A., and Wittrock, F.: REanalysis of the TROpospheric chemical composition over the past 40 years (RETRO) - A long-term global modeling study of tropospheric chemistry, Report No. 48/2007, Reports on Earth System Science, Max Planck Institute for Meteorology, Julich/Hamburg, Germany, 2007.

Streets, D. G., Yarber, K. F., Woo, J. H., and Carmichael, G. R.: Biomass burning in Asia: Annual and seasonal estimates and atmospheric emissions, Global Biogeochem. Cy., 17, 1099, doi:10.1029/2003GB002040, 2003a.

Streets, D. G., Bond, T. C., Carmichael, G. R., Fernandes, S. D., Fu, Q., He, D., Klimont, Z., Nelson, S. M., Tsai, N. Y., Wang, M. Q., Woo, J.-H., and Yarber, K. F.: An inventory of gaseous and primary aerosol emissions in Asia in the year 2000, J. Geophys. Res., 108, 8809, doi:10.1029/2002JD003093, 2003b.

Tosca, M. G., Randerson, J. T., Zender, C. S., Nelson, D. L., Diner, D. J., and Logan, J. A.: Dynamics of fire plumes and smoke clouds associated with peat and deforestation fires in Indonesia, J. Geophys. Res., 116, D08207, doi:10.1029/2010JD015148, 2011.





ACPD
13, 23781–23816, 2013



Turquety, S., Logan, J. A., Jacob, D. J., Hudman, R. C., Leung, F. Y., Heald, C. L., Yantosca, R. M., Wu, S. L., Emmons, L. K., Edwards, D. P., and Sachse, G. W.: Inventory of boreal fire emissions for North America in 2004: Importance of peat burning and pyroconvective injection, J. Geophys. Res., 112, 1–13, doi:10.1029/2006JD007281, 2007.

Val Martin, M., Logan, J. A., Kahn, R. A., Leung, F. Y., Nelson, D. L., and Diner, D. J.: Smoke injection heights from fires in North America: analysis of 5 years of satellite observations, Atmos. Chem. Phys., 10, 1491–1510, doi:10.5194/acp-10-1491-2010, 2010.

Val Martin, M., Kahn, R. A., Logan, J. A., Paugam, R., Wooster, M., and Ichoku, C.: Space-based observational constraints for 1-D fire smoke plume-rise models, J. Geophys. Res., 117, D22204, doi:10.1029/2012jd018370, 2012.

van der Werf, G. R., Randerson, J. T., Giglio, L., Collatz, G. J., Kasibhatla, P. S., and Arellano, A. F.: Interannual variability in global biomass burning emissions from 1997 to 2004, Atmos. Chem. Phys., 6, 3423–3441, doi:10.5194/acp-6-3423-2006, 2006.

Wang, Y. H., Jacob, D. J., and Logan, J. A.: Global simulation of tropospheric $O_3$-$NO_x$-hydrocarbon chemistry 1. Model formulation, J. Geophys. Res., 103, 10713–10725, doi:10.1029/98JD00158, 1998.

Wesely, M. L.: Parameterization of surface resistances to gaseous dry deposition in regional-scale numerical models, Atmos Environ, 23, 1293–1304, doi:10.1016/0004-6981(89)90153-4, 1989.

Wu, S, Mickley, L. J., Jacob, D. J., Logan, J. A., and Yantosca, R. M.: Why are there large differences between models in global budgets of tropospheric ozone?, J. Geophys. Res, 112, D05302, doi:10.1029/2006JD007801, 2007.

Yen, M.-C., Peng, C.-M., Chen, T.-C., Chen, C.-S., Lin, N.-H., Tzeng, R.-Y., Lee, Y.-A., and Lin, C.-C.: Climate and weather characteristics in association with the active fires in northern Southeast Asia and spring air pollution in Taiwan during 2010 7-SEAS/Dongsha Experiment, Atmos. Environ., doi:10.1016/j.atmosenv.2012.11.015, 2012.

Zender, C. S., Krolewski, A. G., Tosca, M. G., and Randerson, J. T.: Tropical biomass burning smoke plume size, shape, reflectance, and age based on 2001-2009 MISR imagery of Borneo, Atmos. Chem. Phys., 12, 3437–3454, doi:10.5194/acp-12-3437-2012, 2012.

Zhang, L., Jacob, D. J., Boersma, K. F., Jaffe, D. A., Olson, J. R., Bowman, K. W., Worden, J. R., Thompson, A. M., Avery, M. A., Cohen, R. C., Dibb, J. E., Flock, F. M., Fuelberg, H. E., Huey, L. G., McMillan, W. W., Singh, H. B., and Weinheimer, A. J.: Transpacific transport of ozone pollution and the effect of recent Asian emission increases on air quality in North America:





ACPD
13, 23781–23816, 2013



an integrated analysis using satellite, aircraft, ozonesonde, and surface observations, Atmos. Chem. Phys., 8, 6117–6136, doi:10.5194/acp-8-6117-2008, 2008.
Zhang, Q., Streets, D. G., Carmichael, G. R., He, K., Huo, H., Kannari, A., Klimont, Z., Park, I., Reddy, S., and Fu, J.: Asian emissions in 2006 for the NASA INTEX-B mission, Atmos. Chem. Phys., 9, 5131–5153, doi:10.5194/acp-9-5131-2009, 2009.





ACPD
13, 23781–23816, 2013



**Table 1.** Annual biomass burning and anthropogenic emissions from the PSEA[a] and from the entire East and South Asia[b].

| | Biomass burning[c] | | Anthropogenic activities[d] | |
|---|---|---|---|---|
| | PSEA | East and South Asia | PSEA | East and South Asia |
| CO [Tg yr$^{-1}$] | 32 | 67 | 21 | 300 |
| BC [TgC yr$^{-1}$] | 0.21 | 0.45 | 0.18 | 3.0 |
| $NO_x$ [TgN yr$^{-1}$] | 0.33 | 0.85 | 0.58 | 11 |
| NMVOC [TgC yr$^{-1}$] | 5.7 | 12 | 5.0 | 55 |

[a] Here defined as Vietnam, Cambodia, Thailand, Laos, and Myanmar;
[b] Domain as defined in Fig. 3;
[c] From Streets et al. (2003);
[d] From Zhang et al. (2009) and include biofuel emissions.





ACPD
13, 23781–23816, 2013



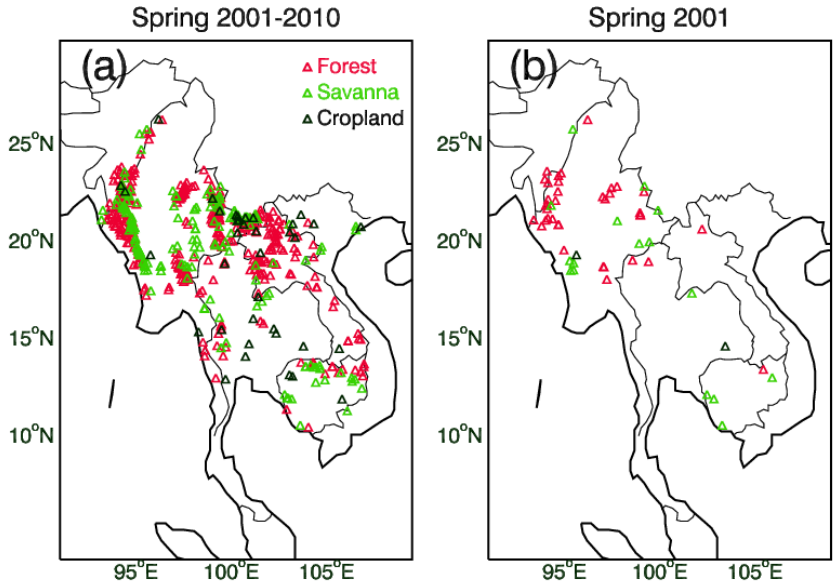


**Fig. 1.** Locations of identified smoke plumes over the PSEA during February–April **(a)** for the years 2001 to 2010 and **(b)** for the year 2001. Symbols represent plumes over evergreen and deciduous broadleaf forest (red), woody savanna (green), and cropland and cropland/natural vegetation mosaics (black), respectively.





ACPD
13, 23781–23816, 2013

Injection heights of springtime biomass burning plumes

Y. Jian and T.-M. Fu



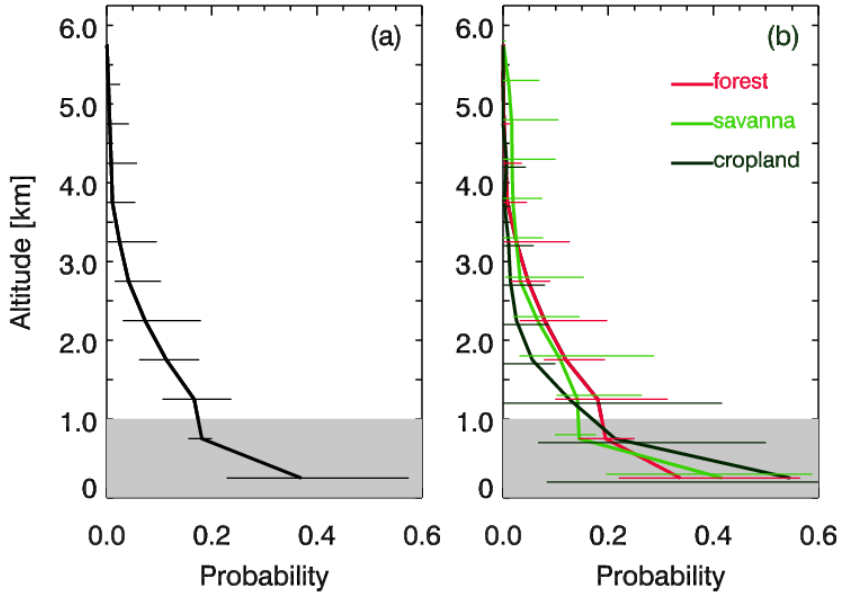


**Fig. 2. (a)** Probability distribution of smoke pixel heights from smoke plumes observed by MISR during February to April for the years 2001-2010. The grey area below 1 km altitude indicates the mean local boundary layer at Terra overpass time (10:30 LT) in the MERRA assimilated meteorology dataset. The error bars show the range of probability for individual years between 2001 and 2010. **(b)** Probability distributions for smoke pixel heights associated with different land covers: evergreen and deciduous broadleaf forest (red), woody savanna (green), and cropland and cropland/natural vegetation mosaic (black). The error bars show the range of probabilities for individual years.





ACPD
13, 23781–23816, 2013



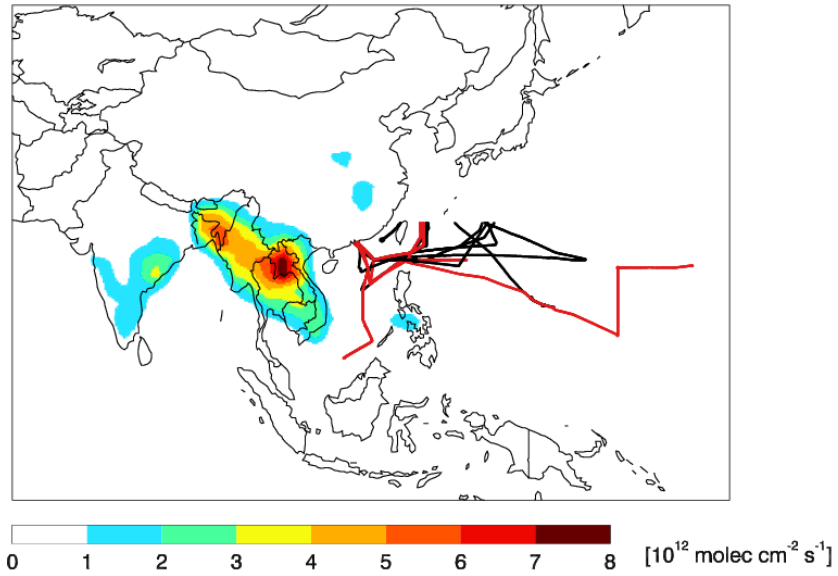


**Fig. 3.** Biomass burning emissions of CO from East and South Asia for March 2001. The emission fluxes were from the inventory developed by Streets et al. (2003). Also shown are the locations of the BC measurements over the northwestern Pacific from the Trace-P aircraft campaign which we used for model evaluation in Sect. 5 (black lines: DC-8; red lines: P-3B).





ACPD
13, 23781–23816, 2013



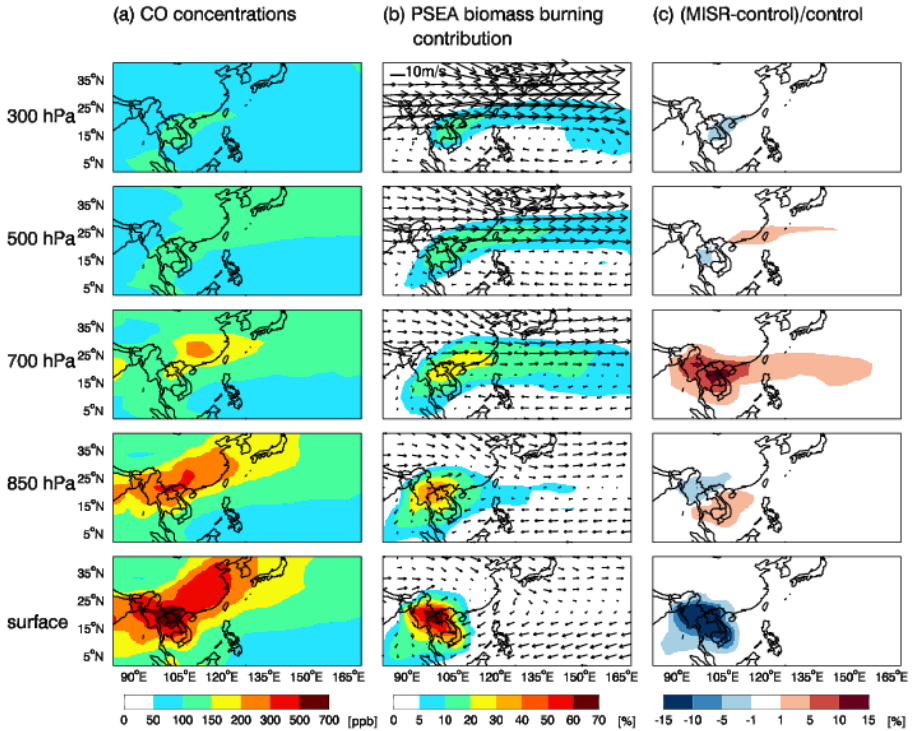


**Fig. 4. (a)** Monthly mean CO concentrations and **(b)** the fractions contributed by biomass burning from the PSEA at five different altitudes during March 2001 in the control simulation. Arrows indicate the monthly mean wind. **(c)** The percent changes of simulated monthly mean CO concentrations in the MISR-constrained simulation relative to the control simulation.





ACPD
13, 23781–23816, 2013

Injection heights of springtime biomass burning plumes

Y. Jian and T.-M. Fu



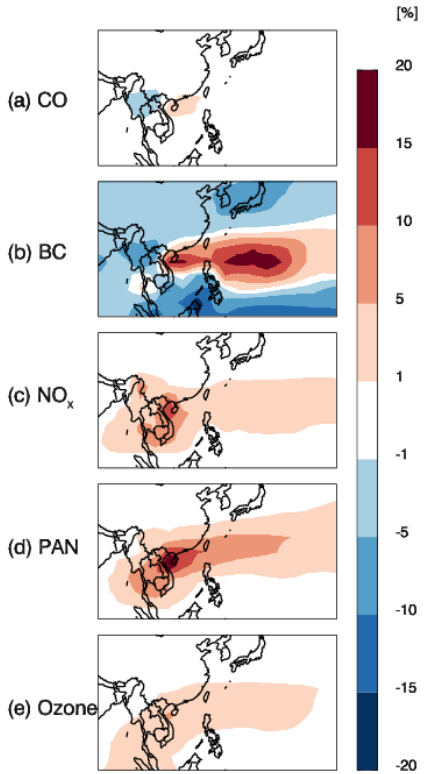


**Fig. 5.** Percent differences of tropospheric column **(a)** CO, **(b)** BC, **(c)** $NO_x$, **(d)** PAN, and **(e)** ozone concentrations in the MISR-constrained simulation relative to control simulation during March 2001.





ACPD
13, 23781–23816, 2013



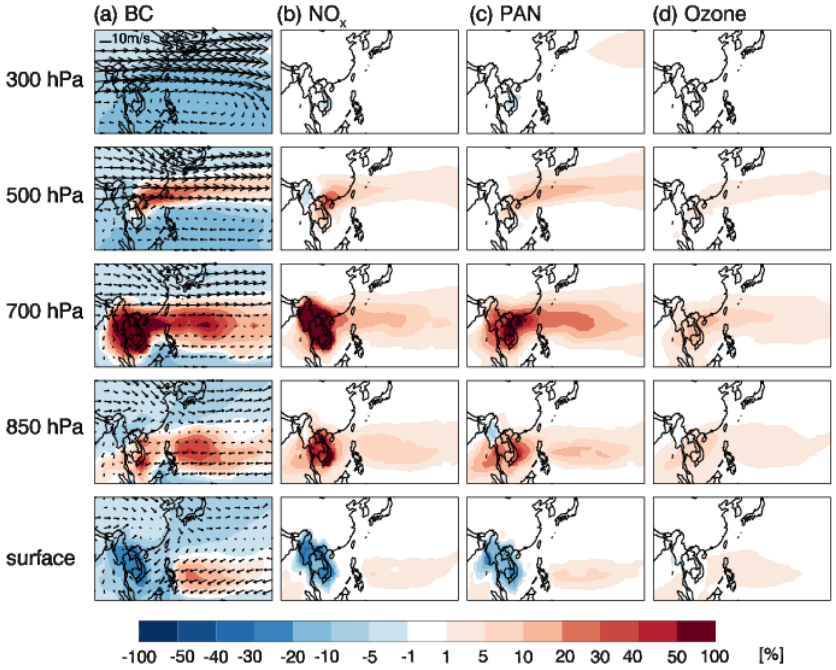


**Fig. 6.** Percent changes of pollutant concentrations in the MISR-constrained simulation relative to the control simulation for **(a)** BC, **(b)** $NO_x$, **(c)** PAN, and **(d)** ozone at five altitudes during March 2001. Arrows indicate the monthly mean wind.





ACPD
13, 23781–23816, 2013



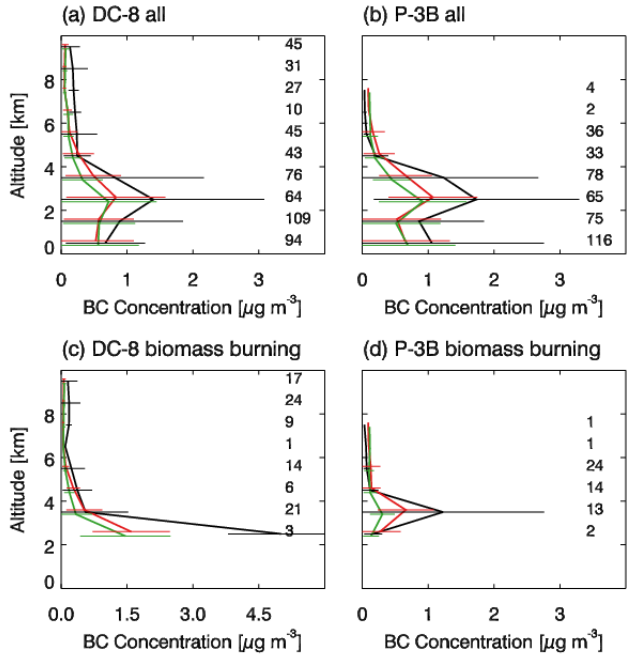


**Fig. 7.** Vertical profiles of BC concentrations over the northwestern Pacific (south of 25° N) as measured by aircrafts during the TRACE-P campaign and as simulated by the model. The black, red and green lines represent BC concentrations from the aircraft observations, the sensitivity simulation using the MISR injection height profile, and the control simulation, respectively. **(a, b)**: all air masses sampled by the TRACE-P aircrafts (DC-8 and P-3B). **(c, d)**: air masses significantly impacted by biomass burning. Model results were sampled along the flight tracks (Fig. 3). Measurements and model results were both averaged to the temporal and spatial resolution of the model for comparison. The error bars show the standard deviations. The numbers on the right are the numbers of model grids averaged.





ACPD
13, 23781–23816, 2013

Injection heights of springtime biomass burning plumes

Y. Jian and T.-M. Fu